ACS Photonics

pubs.acs.org/journal/apchd5

Article

Microfiber Mechanical Resonator for Optomechanics

Qiang Zhang, Ruili Zhai, Shiwei Yang, Shuai Yang, and Yongmin Li*

Cite This: *ACS Photonics* 2020, 7, 695−700

Read Online

ACCESS | Metrics & More | Article Recommendations

ABSTRACT: Optomechanics is a promising field with important applications in ultrasensitive sensing and quantum information processing. A variety of micromechanical resonators are proposed and demonstrated for expanding the applications of optomechanical technologies. In this paper, we report a novel microfiber mechanical resonator. By designing abrupt junctions between the microfiber and single mode fibers and imposing high axial stress in the resonator, the clamping loss is decreased effectively and the resonator material's intrinsic dissipation is also diluted. Ringdown measurements at room temperature show that the quality factors Q_m of the fundamental and higher-order mechanical modes of the microfiber resonators exceed 10^5 to yield the highest mechanical $f \times Q_m$ products ($>10^{10}$ Hz) yet reported for fiber-optic mechanical resonators. Moreover, employing the microfiber as a vibrating beam, the mass of the resonator is at least 1 order of magnitude less than that of the reported fiber-optic resonators with a similar $f \times Q_m$ product. The proposed mechanical resonator is a promising candidate for optomechanics and provides an alternative mechanism for optical fiber sensing and communication systems.

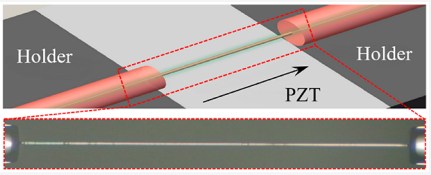

KEYWORDS: *fiber optics, optomechanics, strain, resonators, heterodyne*

Optomechanical systems have emerged as powerful platforms for various classical and quantum applications and offer tremendous advantages for integrated quantum systems.[1,2] Some quantum phenomena in optomechanical systems have been demonstrated, such as ground state cooling of mechanical resonators,[3−5] squeezing,[6−13] and entanglement[14−16] for light and mechanical resonators. The quantum optomechanical systems operating at room temperature are advantageous for practical applications. However, they require the $f \times Q_m$ product of the mechanical resonators larger than the value of $k_B T_{room}/h$,[17] where f is the resonant frequency, Q_m is the mechanical quality factor, T_{room} is the room temperature, and h and k_B are the Planck and the Boltzmann constants, respectively. The mechanical resonators with high $f \times Q_m$ product become a major challenge for building realistic quantum optomechanics systems at room temperature.[18−24]

To expand optomechanical technologies, a number of novel optomechanical devices have been reported over the past few years, such as bulk acoustic resonator,[25] superfluid liquid helium,[26,27] droplet cavities,[28] swept-frequency resonators,[29] single-crystal diamond resonators,[30,31] and fiber-optic resonators.[32−36] Fiber-optic optomechanical technologies present alternative mechanisms for optical fiber sensing and communication systems. Previous works on fiber-optic mechanical resonators mainly focused on tapered optical fibers.[32−36] The exponential radius profile of the tapered optical fibers confines the phonons to the nanofiber waist to work as mechanical resonators. The $f \times Q_m$ maxima of the torsional[32] and flexural[34] modes of the reported taper-fiber resonators are 10^9 and 10^8, respectively.

In this work, we present a microfiber mechanical resonator for optomechanics. The proposed device is fabricated by splicing a microfiber between two single mode fibers (SMFs). Compared with the taper sections, the abrupt junctions between the microfiber and SMFs could effectively suppress clamping loss. The clamped−clamped fixation method not only increases the resonant frequency but also provides an approach to optimize further the characteristic parameters of the resonators by applying an axial stress. The high stress from an axial strain by a piezoelectric stack (PZT) strongly decreases the bending and clamping losses by reducing the vibration mode's curvature, and it also increases the mechanical resonant frequency. In our experiments, the $f \times Q_m$ maxima of the fundamental and higher-order mechanical modes of the microfiber resonators are both larger than 10^{10}. Moreover, the mass of the microfiber resonator is at least 1 order of magnitude less than that of the reported taper-fiber resonator, which could be beneficial for improving the single-photon coupling strength in optomechanical systems. These advantages make the proposed microfiber resonator an attractive mechanical resonator for optomechanical applications, and it presents an alternative mechanism for optical fiber sensing and communication systems.

Received: October 28, 2019
Published: February 4, 2020

FABRICATION

The fabrication process of the microfiber resonator is shown in Figure 1a. First, the microfiber with suitable diameters is produced by the drawing of SMFs on a scanning oxyhydrogen flame, where the parameters of the microfiber could be controlled flexibly by adjusting the pulling speed and temperature of the oxyhydrogen flame. Second, the microfiber is cleaved by a fiber-optic cleaver (S326, FITEL) at the uniform waist and spliced to a SMF. A large offset has to be set in the splicing process of the microfiber and SMF to avoid the deformation of the microfiber, and this offset is 300 μm for the fusion splicer machine (S183 ver. 2, FITEL) in our experiments. Then, the microfiber is cleaved again with a designed length and spliced with another SMF. It should be noted that the end faces of the microfiber need to be flat and smooth, which determine the mechanical performance of the splicing spots and the clamping loss of the mechanical resonator. Figure 1b shows the image of a microfiber mechanical resonator, where the length and diameter of the microfiber are 950 and 13 μm, respectively. Here, the abrupt junctions between the microfiber and SMFs are used to replace the taper sections to reduce the clamping loss.

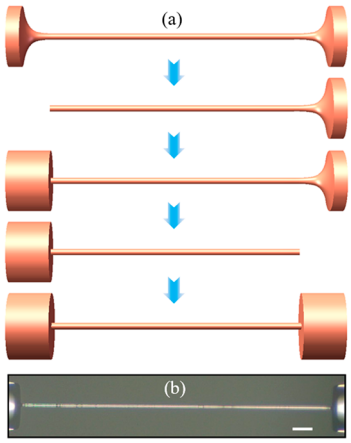

Figure 1. (a) Schematic of the fabrication process of the microfiber resonator. (b) Optical micrograph of the microfiber resonator. The white scale bar at the lower right corner is 50 μm.

RESULTS AND DISCUSSION

Figure 2a shows a scheme of the experimental setup for characterizing the microfiber resonator by performing a heterodyne detection. Pump light (with a wavelength of 1550 nm) modulated by a Mach-Zehder intensity modulator (with an extinction ratio of 26 dB) with a square-wave signal is injected into the microfiber resonator to excite the harmonic modes of the resonator,[33] and it is then eliminated by the filter. Probe light (with a wavelength of 1539.766 nm) from a continuous-wave tunable laser is split into two beams using a 90/10 fiber coupler. One beam is sent to an acousto-optic frequency shifter (80-MHz blueshift), fiber polarization controller, and variable optical attenuator and used as an optical local oscillator for heterodyne detection. The other beam is coupled into the microfiber resonator under test. The light through the microfiber resonator is then combined with the optical local oscillator using a 50/50 optical coupler to produce an optical beat note on a fast photodetector, and the signals of interest are converted to radio frequency signals (80 MHz $\pm$ f_n), which are recorded with an electrical spectrum analyzer. The resonant frequency of the microfiber resonator could be influenced by the gas pressure in the vacuum chamber and the continuous-wave light power.[34] In our experiments,

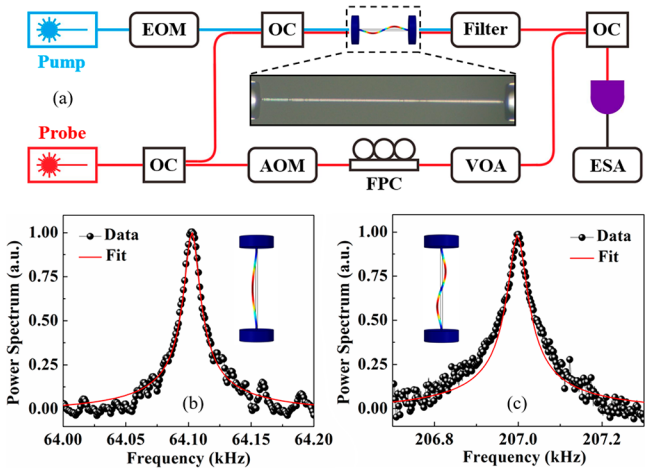

Figure 2. (a) Schematic of the experimental setup, including an electro-optic modulator (EOM), optical coupler (OC), vacuum chamber (VC), acousto-optic modulator (AOM), fiber polarization controller (FPC), variable optical attenuator (VOA), and electrical spectrum analyzer (ESA). (b and c) Normalized mechanical power spectra of the first and second modes for the microfiber mechanical resonator. Inset: Mode shapes of the first and second modes.

the gas pressure in the vacuum chamber is kept at 5×10^{-7} mbar, and the power of the probe light through the resonator is kept low at 10 μW to remove their influence on the resonant frequency.

Figure 2b,c plots the measured first mode and second mode mechanical power spectra of the microfiber resonator with a length of 950 μm and diameter of 13 μm in the relaxed state by scanning the vibrational frequency. The black points represent data measured in the experiments, and the red solid line is fitted according to the response function of the mechanical resonator. The resonant frequency f_1 and line width Γ_1 of the first mode are 64.102 kHz and 12 Hz, and the corresponding Q_1 factor is f_1/Γ_1 = 5300. The second mode has a resonant frequency f_2 = 206.997 kHz and line width Γ_2 = 45 Hz, and the corresponding Q_2 factor is 4600. The insets in Figure 2 are the mode shapes of the two resonant modes.

The $f \times Q_m$ product is a significant parameter for the mechanical resonator in optomechanical systems. Various methods have been proposed to improve the effective resonant frequencies and quality factors of mechanical resonators,[37] such as feedback control, optical or mechanical pumping, axial stress, and parametric pumping. Compared to cantilever mechanical resonators, a clamped−clamped microfiber resonator offers a convenient approach to impose axial tensile strain on the resonator, which is an effective method to enhance the resonant frequency and quality factor of the resonator.[38−40] As shown in Figure 3, the axial tensile strain is applied directly to the resonator by a PZT. When the tensile

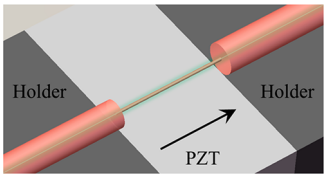

Figure 3. Elastic strain model of the microfiber mechanical resonator in the axial tensile state. The black arrow points to the direction of the axial strain.

https://dx.doi.org/10.1021/acsphotonics.9b01560
ACS Photonics 2020, 7, 695−700

strain ΔL is applied to the resonator, the length of the microfiber becomes $L = L_0 + \Delta L$, and the diameter of the microfiber becomes $r = r_0\ (1 - \gamma \Delta L/L_0)$, where the γ is the Poisson ratio, and L_0 and r_0 are the primary length and diameter of the resonator, respectively. The changes of the length and diameter have not been considered in the traditional model under axial loads[40] and need to be considered for this resonator. According to Euler−Bernoulli beam theory,[41,42] the nth resonant frequency f_n of the microfiber resonator under tensile axial strain ΔL can be expressed as

$$f_n(\Delta L) = \frac{(2n+1)^2\pi(\gamma L_0 - \Delta L)r_0}{16\gamma L_0(L_0+\Delta L)^2} \times \sqrt{\frac{E}{\rho}\left(1 + \frac{4\Delta L L_0 \gamma^2 (L_0+\Delta L)^2}{n^2\pi^2 r_0^2(\gamma L_0 - \Delta L)^2}\right)} \quad (1)$$

where the E is the Young's modulus of the microfiber and ρ is the mass density of the microfiber.

In our experiments, the response of the microfiber resonator is characterized as the axial tensile strain is tuned by using a PZT, where the length response of the PZT as a function of the applied voltage V is $\Delta L = 0.33 \times 10^{-9} \times V^{1.3}$. As shown in Figure 4, the solid lines represent the measured normalized

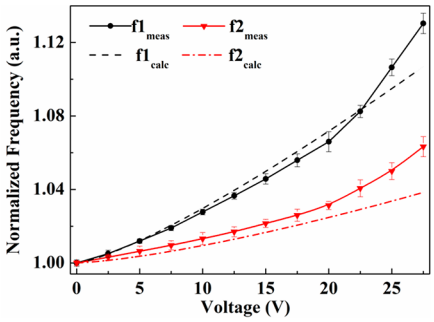

Figure 4. Measured and calculated normalized mechanical resonant frequencies of the microfiber resonator as a function of voltage on the PZT.

resonant frequency shifts as the voltage applied to the PZT, and the dashed lines represent the calculated normalized resonant frequency shifts according to the eq 1, where the Young's modulus E is 73 GPa and the mass density ρ is 2320 kg/m^3. The experimental results show that the resonant frequency f_1 and f_2 increase, and the increasing extent of the first mode is larger than that of the second mode as the voltage V on the PZT, which is in good agreement with the calculated curves. In contrast to the length increase of the resonator that results in the reduction of the resonant frequency, the axial stress dominates the resonant frequency shifts under an axial tensile stress for the proposed device. The difference between the measured shifts and the calculated shifts probably arises from small disagreements between the measured values and real devices' geometry and the material values, as well as the noncircular microfiber cross section.

The quality factor of a mechanical resonator characterizes the ratio of total stored energy in a resonator relative to the lost energy during one vibrating cycle. For a micro-string resonator,[43] the quality factor of micro-strings is mainly limited by bending losses in the relaxed state. The deflection of the mechanical resonator with same kinetic energy in the tensile state is less than that in the relaxed state. Thus, the corresponding bending loss decreases and the quality factor is enhanced by applying the axial tensile stress to the resonator. One can express the quality factor Q_{strain} of the microfiber resonator in tensile state as

$$\frac{Q_{strain}}{Q_{bend}} = 1 + \left[\frac{n^2\pi r_0^2(L_0 - \gamma\Delta L)^2}{8L_0\Delta L(L_0+\Delta L)^2} + \frac{r_0(L_0 - \gamma\Delta L)\sqrt{2\Delta L/L_0}}{3\pi\Delta L(L_0+\Delta L)}\right]^{-1} \quad (2)$$

where Q_{bend} is the quality factor due to the bending related damping mechanisms in the relaxed state.

In our experiments, we also assess the change of the quality factor of the microfiber mechanical resonator under the axial tensile strain. Figure 5 shows the corresponding response of

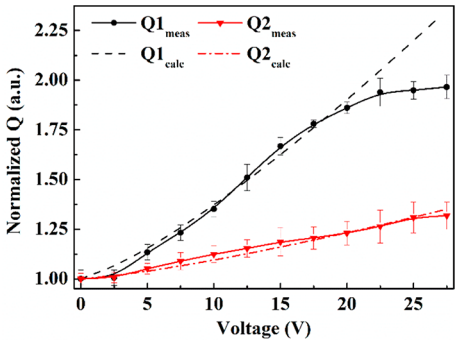

Figure 5. Measured and calculated normalized quality factors of the microfiber resonator as a function of the voltage on the PZT.

the quality factor of the microfiber resonator as the voltage increases on the PZT. The solid lines represent the measured normalized quality factors, and the dashed lines represent the calculated normalized quality factors according to eq 2. For a micro-string resonator,[43] the bending loss dominates the mechanical dissipation in the beginning and decreases by imposing an axial tensile strain because of the reduction of the deflection. Therefore, the quality factors of the two resonant modes are enhanced by the axial tensile strain as the voltage increases as shown in Figure 5. The increasing extent of the quality factor is in inverse proportion to the n_2 according to eq 2, so the increasing extent of the first mode is larger than that of the second mode similar to the resonant frequency response, which is consistent with the measured experimental data. When the axial tensile strain is big enough, the bending loss is not the dominating mechanical dissipation, the influence of the tensile strain decreases, and the quality factor of the resonator becomes saturated.

To corroborate the mechanical properties of the proposed clamped−clamped flexural microfiber mechanical resonators, we have fabricated many of the proposed devices with varying geometrical parameters and axial tensile stresses. Table 1 shows the first four order resonant frequencies and the quality factors of six resonators having different geometrical parameters and tensile strain. The experimental results show that the $f \times Q_m$ products of the fundamental modes for all of the resonators are larger than 10^8, and the maximum of the $f \times Q_m$ product for the fundamental mode is 1.45×10^{10} for the resonator with a length of 5920 μm. For the higher-order mechanical modes, the $f \times Q_m$ maximum is 1.97×10^{10} for the third mode of the resonator with a length of 5920 μm. The corresponding ringdown measurements for the best observed

https://dx.doi.org/10.1021/acsphotonics.9b01560
ACS Photonics 2020, 7, 695−700

Table 1. Resonant Frequencies f_n (kHz) and Quality Factors Q_n of Microfiber Resonators with Different Geometrical Parameters L_0 (μm), r_0 (μm), and Tensile Strains ΔL (nm)

L_0	r_0	ΔL	f_1	Q_1	f_2	Q_2	f_3	Q_3	f_4	Q_4
844	10	554	202	2000	307	200	535	3200	771	4500
1156	9	427	103	2900	179	15200	252	16800	388	10200
1367	10	711	106	16300	171	17300	215	7100	335	1600
4012	10	2198	38	25600	45	7300	78	11000	91	4600
4810	9	2108	26.7	183600	38.5	127700	52.5	140100	64.2	89300
5920	10	1622	16.5	880500	25	487900	32.9	601600	41.2	256400

values for fundamental and higher-order modes are shown in Figure 6.

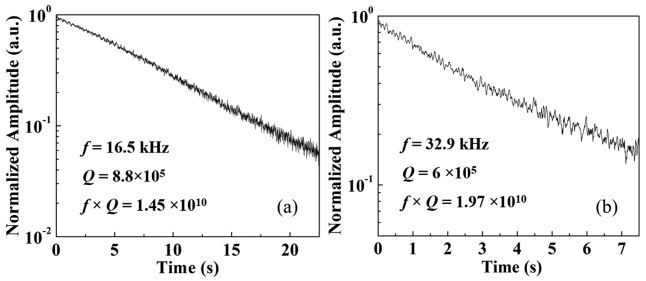

Figure 6. Ringdown measurements for the best observed values for the fundamental (a) and higher-order (b) modes.

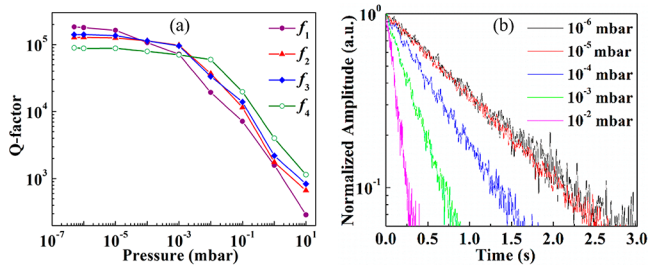

Figure 7. (a) Q_m factors of the different mechanical modes as a function of the gas pressure for the microfiber resonator with a length of 4810 μm. (b) Corresponding ringdown results of the fundamental modes.

It is meaningful to explore the theoretical limits of the $f \times Q_m$ product for the proposed microfiber mechanical resonator in ideal conditions. According to the optimizing mechanism of the bending loss by applying an axial strain, the resonant frequency f and the Q_m factor will increase continuously as the axial strain increases. In our experiment, the axial tensile strain applied to the resonator is far less than the reported rupture strain[44] due to the limit of the PZT used. The theoretical maximum values of the f and the Q_m factor for the mechanical resonator with a length of 5920 μm are 268.5 kHz and 2.7×10^7, and the corresponding $f \times Q_m$ is 7.25×10^{12}. In the above analysis, we have neglected clamping loss and thermoelastic loss, since the theoretical models of the clamping[45,46] and thermoelastic[47,48] losses predict that the limited Q_m factors are about 10^7 and 10^8 for the microfiber mechanical resonator with a length of 5920 μm, respectively, and both of them could be suppressed as the increase of the axial strain because of the decrease of the vibration amplitude. In addition, the experiment showed that the surface loss resulted from the surface defects and absorbates is one of the dominating losses for nanometer resonators rather than for micrometer resonators and can be suppressed effectively by annealing treatment.[49] The smooth surface of the microfiber by drawing of SMFs on an oxyhydrogen flame is beneficial to reduce the surface loss. Therefore, it is possible to use the microfiber mechanical resonator as a room temperature optomechanical system. Besides relying on increasing the axial strain, other methods for further optimizing the proposed device will also be pursued in our future work, such as increasing the difference of the diameters between the SMFs and microfiber and fabricating periodic microstructure on the microfiber like in ref 23.

We also investigate the response of the Q_m factor to air damping. As shown in Figure 7a, the Q_m factors become saturated when the gas pressure is less than 10^{-5} mbar. The air damping dominates the Q_m factors when the gas pressure is higher than 10^{-5} mbar. Figure 7b plots the corresponding ringdown measurement results of the fundamental modes with different gas pressures from 10^{-6} mbar to 10^{-2} mbar.

In addition to the higher $f \times Q_m$ product for the proposed clamped−clamped microfiber mechanical resonator, another advantage is the smaller mass, which is a crucial parameter for mechanical resonators with respect to improving the single-photon coupling strength in optomechanical experiments. In our experiments, the mass of the microfiber resonator with a $f \times Q_m$ product similar to that of the taper-fiber resonator is at least 1 order of magnitude smaller than that of the taper-fiber resonator because the length and diameter of the microfiber are much less than those of the taper fiber. Therefore, the microfiber resonator is a promising candidate for fiber-optic optomechanical systems.

For optomechanical systems, the optomechanical coupling rate g_{om} is one of the key parameters, which represents the optical frequency shift per displacement. The microfiber mechanical resonator could couple with a whispering-gallery mode cavity. According to the dispersive optomechanical coupling configuration and theory,[50] the optomechanical coupling rate g_{om} for the resonator with a length of 950 μm and diameter of 13 μm is about 4 MHz/nm. One of our future works is to explore the interaction between the proposed microfiber mechanical resonator and a whispering-gallery mode cavity.

The high-Q_m mechanical resonators could be used not only in optomechanics but also in ultrasensitive detection by monitoring the variations of the resonant peak, such as shifting, splitting, and broadening. Various systems with exquisite sensitivity have been proposed to measure displacement,[51] temperature,[52] single-spin,[53] and single-protein mass spectrometry.[54] Compared with other mechanical resonators, the microfiber mechanical resonator does not need an additional optical system to read out the mechanical motion of the mechanical resonators, which is beneficial to simplify the detection systems.

https://dx.doi.org/10.1021/acsphotonics.9b01560
ACS Photonics 2020, 7, 695−700

CONCLUSION

In summary, we have proposed and demonstrated a novel type of fiber-optic mechanical resonator by splicing a microfiber between two SMFs. By designing abrupt junctions between the microfiber and the SMFs and imposing high axial stress in the resonator, the clamping loss and material's intrinsic dissipation are both reduced effectively, and thus the $f \times Q_m$ product is improved. In addition, the mass of this device is far less than that of the reported other fiber-optic resonators. The high $f \times Q_m$ product and small mass make it a promising platform for optomechanical systems. Furthermore, the proposed device also offers a novel working mechanism for optical fiber technologies and has the potential to expand the optical fiber technologies in the area of ultrasensitive detection.

AUTHOR INFORMATION

Corresponding Author

Yongmin Li − *State Key Laboratory of Quantum Optics and Quantum Optics Devices, Institute of Optoelectronics and Collaborative Innovation Center of Extreme Optics, Shanxi University, Taiyuan 030006, People's Republic of China*; Email: yongmin@sxu.edu.cn

Authors

Qiang Zhang − *State Key Laboratory of Quantum Optics and Quantum Optics Devices, Institute of Optoelectronics and Collaborative Innovation Center of Extreme Optics, Shanxi University, Taiyuan 030006, People's Republic of China*; orcid.org/0000-0002-9270-9994

Ruili Zhai − *State Key Laboratory of Quantum Optics and Quantum Optics Devices, Institute of Optoelectronics, Shanxi University, Taiyuan 030006, People's Republic of China*

Shiwei Yang − *State Key Laboratory of Quantum Optics and Quantum Optics Devices, Institute of Optoelectronics, Shanxi University, Taiyuan 030006, People's Republic of China*

Shuai Yang − *State Key Laboratory of Quantum Optics and Quantum Optics Devices, Institute of Optoelectronics, Shanxi University, Taiyuan 030006, People's Republic of China*

Complete contact information is available at: https://pubs.acs.org/10.1021/acsphotonics.9b01560

Notes

The authors declare no competing financial interest.

ACKNOWLEDGMENTS

We acknowledge the funding from the National Natural Science Foundation of China (NSFC) (11804208 and 11774209), National Key R&D Program of China (2016YFA0301403), Key Research and Development Projects of Shanxi Province (201803D121065), Applied Basic Research Program of Shanxi Province (201801D221010), and Shanxi 1331KS.

REFERENCES

(1) Aspelmeyer, M.; Kippenberg, T. J.; Marquardt, F. Cavity optomechanics. *Rev. Mod. Phys.* **2014**, *86*, 1391−1452.

(2) Poot, M.; van der Zant, H. S. J. Mechanical systems in the quantum regime. *Phys. Rep.* **2012**, *511*, 273−335.

(3) Park, Y.; Wang, H. Resolved-sideband and cryogenic cooling of an optomechanical resonator. *Nat. Phys.* **2009**, *5*, 489−493.

(4) Chan, J.; Alegre, T. P. M.; Safavi-Naeini, A. H.; Hill, J. T.; Krause, A.; Gröblacher, S.; Aspelmeyer, M.; Painter, O. Laser cooling of a nanomechanical oscillator into its quantum ground state. *Nature* **2011**, *478*, 89−92.

(5) Teufel, J. D.; Donner, T.; Li, D.; Harlow, J. W.; Allman, M. S.; Cicak, K.; Sirois, A. J.; Whittaker, J. D.; Lehnert, K. W.; Simmonds, R. W. Sideband cooling of micromechanical motion to the quantum ground state. *Nature* **2011**, *475*, 359−363.

(6) Szorkovszky, A.; Brawley, G. A.; Doherty, A. C.; Bowen, W. P. Strong Thermomechanical Squeezing via Weak Measurement. *Phys. Rev. Lett.* **2013**, *110*, 184301.

(7) Purdy, T. P.; Yu, P. L.; Peterson, R. W.; Kampel, N. S.; Regal, C. A. Strong Optomechanical Squeezing of Light. *Phys. Rev. X* **2013**, *3*, 031012.

(8) Safavi-Naeini, A. H.; Groblacher, S.; Hill, J. T.; Chan, J.; Aspelmeyer, M.; Painter, O. Squeezed light from a silicon micromechanical resonator. *Nature* **2013**, *500*, 185−189.

(9) Mahboob, I.; Okamoto, H.; Onomitsu, K.; Yamaguchi, H. Two-Mode Thermal-Noise Squeezing in an Electromechanical Resonator. *Phys. Rev. Lett.* **2014**, *113*, 167203.

(10) Wollman, E. E.; Lei, C.; Weinstein, A.; Suh, J.; Kronwald, A.; Marquardt, F.; Clerk, A.; Schwab, K. Quantum squeezing of motion in a mechanical resonator. *Science* **2015**, *349*, 952−955.

(11) Pirkkalainen, J. M.; Damskägg, E.; Brandt, M.; Massel, F.; Sillanpää, M. A. Squeezing of Quantum Noise of Motion in a Micromechanical Resonator. *Phys. Rev. Lett.* **2015**, *115*, 243601.

(12) Lecocq, F.; Clark, J. B.; Simmonds, R. W.; Aumentado, J.; Teufel, J. D. Quantum Nondemolition Measurement of a Nonclassical State of a Massive Object. *Phys. Rev. X* **2015**, *5*, 041037.

(13) Pontin, A.; Bonaldi, M.; Borrielli, A.; Marconi, L.; Marino, F.; Pandraud, G.; Prodi, G. A.; Sarro, P. M.; Serra, E.; Marin, F. Dynamical Two-Mode Squeezing of Thermal Fluctuations in a Cavity Optomechanical System. *Phys. Rev. Lett.* **2016**, *116*, 103601.

(14) Palomaki, T.; Teufel, J.; Simmonds, R.; Lehnert, K. Entangling Mechanical Motion with Microwave Fields. *Science* **2013**, *342*, 710−713.

(15) Riedinger, R.; Wallucks, A.; Marinković, I.; Löschnauer, C.; Aspelmeyer, M.; Hong, S.; Gröblacher, S. Remote quantum entanglement between two micromechanical oscillators. *Nature* **2018**, *556*, 473−477.

(16) Ockeloen-Korppi, C. F.; Damskägg, E.; Pirkkalainen, J. M.; Asjad, M.; Clerk, A. A.; Massel, F.; Woolley, M. J.; Sillanpää, M. A. Stabilized entanglement of massive mechanical Oscillators. *Nature* **2018**, *556*, 478−482.

(17) Marquardt, F.; Chen, J. P.; Clerk, A. A.; Girvin, S. M. Quantum Theory of Cavity-Assisted Sideband Cooling of Mechanical Motion. *Phys. Rev. Lett.* **2007**, *99*, 093902.

(18) Wilson, D. J.; Regal, C. A.; Papp, S. B.; Kimble, H. J. Cavity Optomechanics with Stoichiometric SiN Films. *Phys. Rev. Lett.* **2009**, *103*, 207204.

(19) Chakram, S.; Patil, Y. S.; Chang, L.; Vengalattore, M. Dissipation in Ultrahigh Quality Factor SiN Membrane Resonators. *Phys. Rev. Lett.* **2014**, *112*, 127201.

(20) Norte, R. A.; Moura, J. P.; Gröblacher, S. Mechanical Resonators for Quantum Optomechanics Experiments at Room Temperature. *Phys. Rev. Lett.* **2016**, *116*, 147202.

(21) Reinhardt, C.; Müller, T.; Bourassa, A.; Sankey, J. C. Ultralow-Noise SiN Trampoline Resonators for Sensing and Optomechanics. *Phys. Rev. X* **2016**, *6*, 021001.

(22) Tsaturyan, Y.; Barg, A.; Polzik, E. S.; Schliesser, A. Ultracoherent nanomechanical resonators via soft clamping and dissipation dilution. *Nat. Nanotechnol.* **2017**, *12*, 776−783.

(23) Ghadimi, A. H.; Fedorov, S. A.; Engelsen, N. J.; Bereyhi, M. J.; Schilling, R.; Wilson, D. J.; Kippenberg, T. J. Elastic strain engineering for ultralow mechanical dissipation. *Science* **2018**, *360*, 764−768.

(24) MacCabe, G. S.; Ren, H.; Luo, J.; Cohen, J. D.; Zhou, H.; Sipahigil, A.; Mirhosseini, M.; Painter, O. Phononic bandgap nano-acoustic cavity with ultralong phonon lifetime. *arxiv (cond-mat)*, 1901.041292019, January 14, 2019.

(25) Renninger, W. H.; Kharel, P.; Behunin, R. O.; Rakich, P. T. Bulk crystalline optomechanics. *Nat. Phys.* **2018**, *14*, 601−607.

(26) McAuslan, D. L.; Harris, G. I.; Baker, C.; Sachkou, Y.; He, X.; Sheridan, E.; Bowen, W. P. Microphotonic forces from superfluid flow. *Phys. Rev. X* **2016**, *6*, 021012.
(27) Kashkanova, A. D.; Shkarin, A. B.; Brown, C. D.; Flowers-Jacobs, N. E.; Childress, L.; Hoch, S. W.; Hohmann, L.; Ott, K.; Reichel, J.; Harris, J. G. E. Superfluid Brillouin optomechanics. *Nat. Phys.* **2017**, *13*, 74−79.
(28) Avino, S.; Krause, A.; Zullo, R.; Giorgini, A.; Malara, P.; De Natale, P.; Loock, H. P.; Gagliardi, G. Direct Sensing in Liquids Using Whispering-Gallery-Mode Droplet Resonators. *Adv. Opt. Mater.* **2014**, *2*, 1155−1159.
(29) St-Gelais, R.; Bernard, S.; Reinhardt, C.; Sankey, J. C. Swept-Frequency Drumhead Optomechanical Resonators. *ACS Photonics* **2019**, *6*, 525−530.
(30) Mitchell, M.; Khanaliloo, B.; Lake, D. P.; Masuda, T.; Hadden, J. P.; Barclay, P. E. Single-crystal diamond low-dissipation cavity optomechanics. *Optica* **2016**, *3*, 963−970.
(31) Lake, D. P.; Mitchell, M.; Kamaliddin, Y.; Barclay, P. E. Optomechanically Induced Transparency and Cooling in Thermally Stable Diamond Microcavities. *ACS Photonics* **2018**, *5*, 782−787.
(32) Wuttke, C.; Cole, G.; Rauschenbeutel, A. Optically active mechanical modes of tapered optical fibers. *Phys. Rev. A: At., Mol., Opt. Phys.* **2013**, *88* (R), 061801.
(33) Fenton, E. F.; Khan, A.; Solano, P.; Orozco, L. A.; Fatemi, F. K. Spin-optomechanical coupling between light and a nanofiber torsional mode. *Opt. Lett.* **2018**, *43*, 1534−1537.
(34) Pennetta, R.; Xie, S.; Russell, P. St. J. Tapered Glass-Fiber Microspike: High-Q Flexural Wave Resonator and Optically Driven Knudsen Pump. *Phys. Rev. Lett.* **2016**, *117*, 273901.
(35) Zeltner, R.; Xie, S.; Pennetta, R.; Russell, P. St.J. Broadband, Lensless, and optomechanically Stabilized Coupling into Microfluidic Hollow-Core Photonic Crystal Fiber Using Glass Nanospike. *ACS Photonics* **2017**, *4*, 378−383.
(36) Pennetta, R.; Xie, S.; Zeltner, R.; Russell, P. St. J. Optomechanical cooling of a glass-fibre nanospike evanescently coupled to a whispering-gallery-mode bottle resonator. *arxiv (physics.optics)*, 1804.091152018, April 24, 2018.
(37) Miller, J. M. L.; Ansari, A.; Heinz, D. B.; Chen, Y.; Flader, I. B.; Shin, D. D.; Villanueva, L. G.; Kenny, T. W. Effective quality factor tuning mechanisms in micromechanical resonators. *Appl. Phys. Rev.* **2018**, *5*, 041307.
(38) Verbridge, S. S.; Parpia, J. M.; Reichenbach, R. B.; Bellan, L. M.; Craighead, H. G. High quality factor resonance at room temperature with nanostrings under high tensile stress. *J. Appl. Phys.* **2006**, *99*, 124304.
(39) Schmid, S.; Hierold, C. Damping mechanisms of single-clamped and prestressed double-clamped resonant polymer microbeams. *J. Appl. Phys.* **2008**, *104*, 093516.
(40) Bokaian, A. Natural frequencies of beams under tensile axial loads. *J. Sound Vib.* **1990**, *142*, 481−498.
(41) Jr, W. W.; Timoshenko, S. P.; Young, D. H. *Vibration Problems in Engineering*; Wiley: Hoboken, NJ, U.S.A., 1990.
(42) Cleland, A. N. *Foundations of Nanomechanics: From Solid-State Theory to Device Applications*; Springer: Berlin, Heidelberg, Germany, 2003.
(43) Schmid, S.; Jensen, K. D.; Nielsen, K. H.; Boisen, A. Damping mechanisms in high-Q micro and nanomechanical string resonators. *Phys. Rev. B: Condens. Matter Mater. Phys.* **2011**, *84*, 165307.
(44) Holleis, S.; Hoinkes, T.; Wuttke, C.; Schneeweiss, P.; Rauschenbeutel, A. Experimental stress−strain analysis of tapered silica optical fibers with nanofiber waist. *Appl. Phys. Lett.* **2014**, *104*, 163109.
(45) Hao, Z.; Erbil, A.; Ayazi, F. An analytical model for support loss in micromachined beam resonators with in-plane flexural vibrations. *Sens. Actuators, A* **2003**, *109*, 156−164.
(46) Yang, J.; Ono, T.; Esashi, M. Energy dissipation in submicrometer thick single-crystal silicon cantilevers. *J. Microelectromech. Syst.* **2002**, *11*, 775−783.
(47) Schmid, S.; Hierold, C. Damping mechanisms of single-clamped and prestressed double-clamped resonant polymer microbeams. *J. Appl. Phys.* **2008**, *104*, 093516.
(48) Lifshitz, R.; Roukes, M. L. Thermoelastic damping in micro- and nanomechanical systems. *Phys. Rev. B: Condens. Matter Mater. Phys.* **2000**, *61*, 5600−5609.
(49) Yasumura, K. Y.; Stowe, T. D.; Chow, E. M.; Pfafman, T.; Kenny, T. W.; Stipe, B. C.; Rugar, D. Quality Factors in Micron- and Submicron-Thick Cantilevers. *J. Microelectromech. Syst.* **2000**, *9*, 117−125.
(50) Anetsberger, G.; Arcizet, O.; Unterreithmeier, Q. P.; Rivière, R.; Schliesser, A.; Weig, E. M.; Kotthaus, J. P.; Kippenberg, T. J. Near-field cavity optomechanics with nanomechanical oscillators. *Nat. Phys.* **2009**, *5*, 909−914.
(51) Vanner, M. R.; Hofer, J.; Cole, G. D.; Aspelmeyer, M. Cooling-by-measurement and mechanical state tomography via pulsed optomechanics. *Nat. Commun.* **2013**, *4*, 2295.
(52) Millen, J.; Deesuwan, T.; Barker, P.; Anders, J. Nanoscale temperature measurements using non-equilibrium Brownian dynamics of a levitated nanosphere. *Nat. Nanotechnol.* **2014**, *9*, 425−429.
(53) Rugar, D.; Budakian, R.; Mamin, H. J.; Chui, B. W. Single spin detection by magnetic resonance force microscopy. *Nature* **2004**, *430*, 329−332.
(54) Hanay, M. S.; Kelber, S.; Naik, A. K.; Chi, D.; Hentz, S.; Bullard, E. C.; Colinet, E.; Duraffourg, L.; Roukes, M. L. Single-protein nanomechanical mass spectrometry in real time. *Nat. Nanotechnol.* **2012**, *7*, 602−608.

https://dx.doi.org/10.1021/acsphotonics.9b01560
ACS Photonics 2020, 7, 695−700